RTAX-S TAMU Single Event Dielectric Rupture

August 8, 2006

J.J. Wang and S. Rezgui
(650) 318-4576
jih-jong.wang@actel.com

I. INTRODUCTION

Single event dielectric rupture (SEDR) was observed during a beam test on RTAX2000S devices. This phenomenon, although it has never been observed in any space-flight data, has been attributed to beam-induced antifuse rupture. The characteristics of the SEDR can be summarized as:

1. The SEDR event is identified by a small permanent jump in the core power supply current (I_{CCA}). Sometimes an I_{CCI} jump occurs simultaneously with an I_{CCA} jump. Since all the antifuses are biased by V_{CCA} only, the probable cause for this I_{CCI} jump is an induced current in the V_{CCI}-powered circuits due to an SEDR in the V_{CCA}-powered array.
2. The threshold LET is very high, in this case approximately 80 MeV•cm^2/mg.
3. The DUT always continues to function after SEDR occurs.
4. In this case only one out of three DUT had SEDR occurring; and it occurred only at V_{CC}+10%.
5. The worst-case incidence angle is 90°, or 0°-tilt.

In this document, the rate of SEDR is estimated for the worst-case space environment. Due to the rarity of the event, it is considered more of an academic curiosity than a practical risk.

II. DUT AND BEAM TEST

The details of the beam test can be found in a report, "RTAXS TAMU Single Event Latch-up Test Report" dated July 12, 2006. This report is available for download from the Actel web site at http://www.actel.com/documents/RTAX-S%20High%20Temp%20SEL.pdf. Table I lists the DUT parameters; Table II lists the test log; and Fig. 1 to Fig. 18 shows the in-flux I_{CC} of each run. SEDR events are identified in Fig. 7 and Fig. 9.

III. RATE CALCULATION

Integral flux hitting on a flat antifuse at all angles

$$= \iint_{sphere-surface} F \bullet \cos\theta \bullet d\Omega$$

$$= 2 \bullet \int_0^{2\pi} \int_0^{\frac{\pi}{2}} F \bullet \sin\theta \bullet \cos\theta \bullet d\theta d\varphi$$

$$= 2\pi \bullet F \ \ (\text{ions}\bullet\text{m}^{-2}\bullet\text{s}^{-1})$$

F is the space integral flux (ions•m^{-2}•sr^{-1}•s^{-1}) that can be simulated by CREME96. Fig. 19 shows the plot of *F* versus LET in a typical environment: geosynchronous orbit, solar minimum activity, and 100-mil Al shielding. Use the worst-case scenario of Fig. 7: four (4) SEDR occurred for total fluence of 10^7 cm^{-2}. The integral flux (*F*) for LET ≥ 80 MeV•cm^2/mg (or 80,000 MeV•cm^2/g in Fig. 19) is 1.5×10^{-8} ions•m^{-2}•sr^{-1}•s^{-1}. The SEDR rate (*R*) for an RTAX2000S device in this space environment is:

$$= [4 \div 10^7 \ (\text{ions}\bullet\text{cm}^{-2})] \times 2\pi \times 1.5 \times 10^{-8} \ (\text{ions}\bullet\text{m}^{-2}\bullet\text{s}^{-1})$$

$$= 3.77 \times 10^{-18} \ \text{s}^{-1}$$

$$= 1.19 \times 10^{-10} \ \text{yr}^{-1}$$

So the mean time between SEDR events is approximately ten-billion years! Note that the majority, ≅99%, of antifuses are not in the critical path; and an antifuse rupture will most likely contribute only a few mA of leakage current.

Several comments about the calculation:

1. The test design is a typical case for SEDR events. The reasons are: the number of unused antifuses is independent of the design because about 95% of antifuses are not used for any design; and always about half of the unused antifuses are biased at V_{CCA} and the other half biased at GND.

2. Ions with LET ≥ Threshold cause SEDR at any incident angles. This causes an over estimate of the rate; in other words, this makes the estimate conservative.
3. Effective LET is not applicable. Ions with LET < Threshold but at an angle other than normal incidence do not cause any SEDR because the normal incidence is the worst case.

Table I DUT parameters

Device	RTAX2000S
Package	CQ352
Foundry	UMC
Technology	0.15 µm CMOS
Die-Lot/Serial Number	D1L9R1: 73026 D1KHN1: 79023, 79102
Quantity Tested	3
IO Configuration	LVTTL
Design	SR_1000_4P_70_sp1

Table II Test Log

Run	DUT	Bias (V) V_{CCI}/V_{CCA}	Temp (°C)	Ion	LET MeV•cm²/mg	Tilt	Flux Ions/cm²/s	Fluence Ions/cm²	File Name	Comments
1	79023	3.7/1.7	125	Au	82.8	0	NA	NA	79023Au1	Run aborted
2	79023	3.7/1.7	125	Au	82.8	0	8.71E+04	9.97E+06	79023Au2	Functional
3	79023	3.3/1.5	125	Au	117.2	45	1.50E+05	9.97E+06	79023Au3	Functional
4	79023	3.6/1.65	125	Au	117.2	45	1.67E+05	1.00E+07	79023Au4	Functional
5	79023	3.3/1.5	125	Au	82.8	0	1.73E+05	1.00E+07	79023Au5	Functional
6	73026	3.3/1.5	125	Au	82.8	0	1.14E+05	9.99E+06	73026Au1	Functional
7	73026	3.6/1.65	125	Au	82.8	0	1.19E+05	9.96E+06	73026Au2	Functional
8	73026	3.3/1.5	125	Au	117.2	45	1.21E+05	9.96E+06	73026Au3	Functional
9	73026	3.6/1.65	125	Au	117.2	45	1.23E+05	1.00E+07	73026Au4	Functional
10	79102	3.3/1.5	125	Au	82.8	0	1.51E+05	1.00E+07	79102Au1	Functional
11	79102	3.6/1.65	125	Au	82.8	0	1.42E+05	9.98E+06	79102Au2	Functional
12	79102	3.3/1.5	125	Au	117.2	45	1.18E+05	1.00E+07	79102Au3	Functional
13	79102	3.6/1.65	125	Au	117.2	45	7.88E+04	9.99E+06	79102Au4	Functional
14	79102	3.6/1.65	125	Xe	69.8	45	1.12E+05	9.97E+06	79102Xe1	Functional
15	79102	3.6/1.65	125	Xe	49.3	0	1.12E+05	9.94E+06	79102Xe2	Functional
16	73026	3.6/1.65	125	Xe	49.3	0	1.11E+05	1.00E+07	73026Xe1	Functional
17	73026	3.6/1.65	125	Xe	69.8	45	1.04E+05	1.00E+07	73026Xe2	Functional
18	79023	3.6/1.65	125	Xe	49.3	0	1.05E+05	9.96E+06	79023Xe1	Functional
19	79023	3.6/1.65	125	Xe	69.8	45	1.12E+04	1.00E+07	79023Xe2	Functional

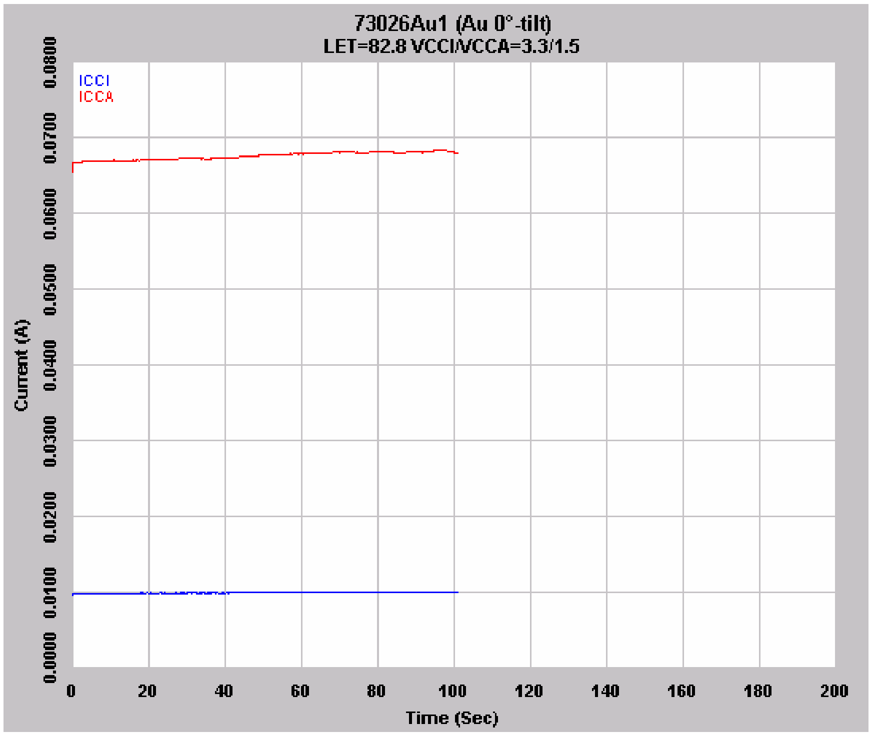

Fig. 1 Plot showing in-flux power supply currents (I_{CCI} and I_{CCA}) of DUT73026 irradiated by Au-ions with 0° tilt; effective LET = 82.8 MeV•cm^2/mg; V_{CCI}/V_{CCA} = 3.3 V/1.5 V

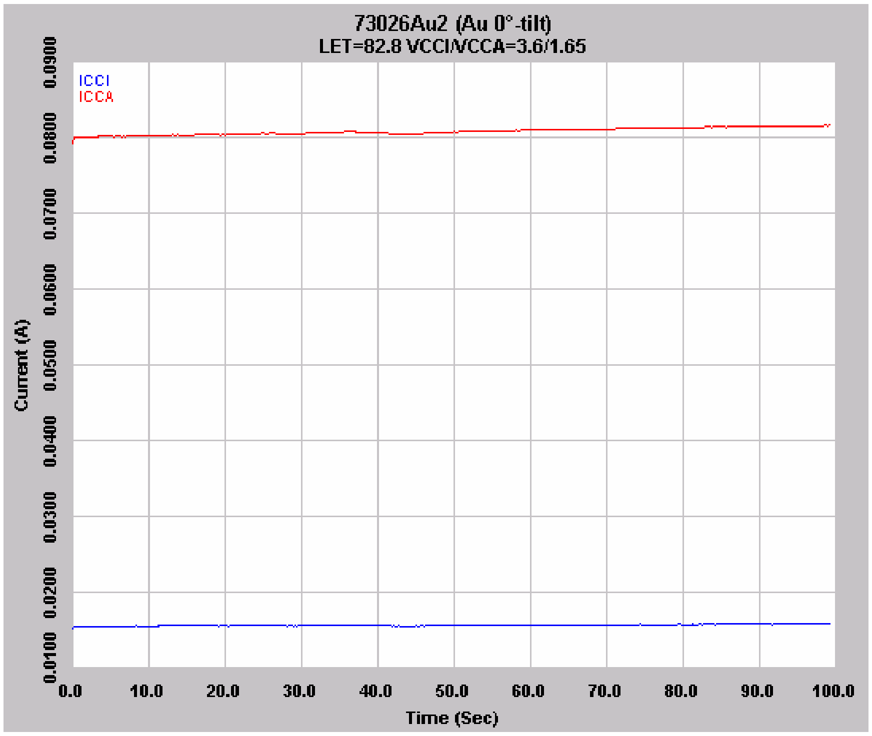

Fig. 2 Plot showing in-flux power supply currents (I_{CCI} and I_{CCA}) of DUT73026 irradiated by Au-ions with 0° tilt; effective LET = 82.8 MeV•cm^2/mg; V_{CCI}/V_{CCA} = 3.6 V/1.65 V.

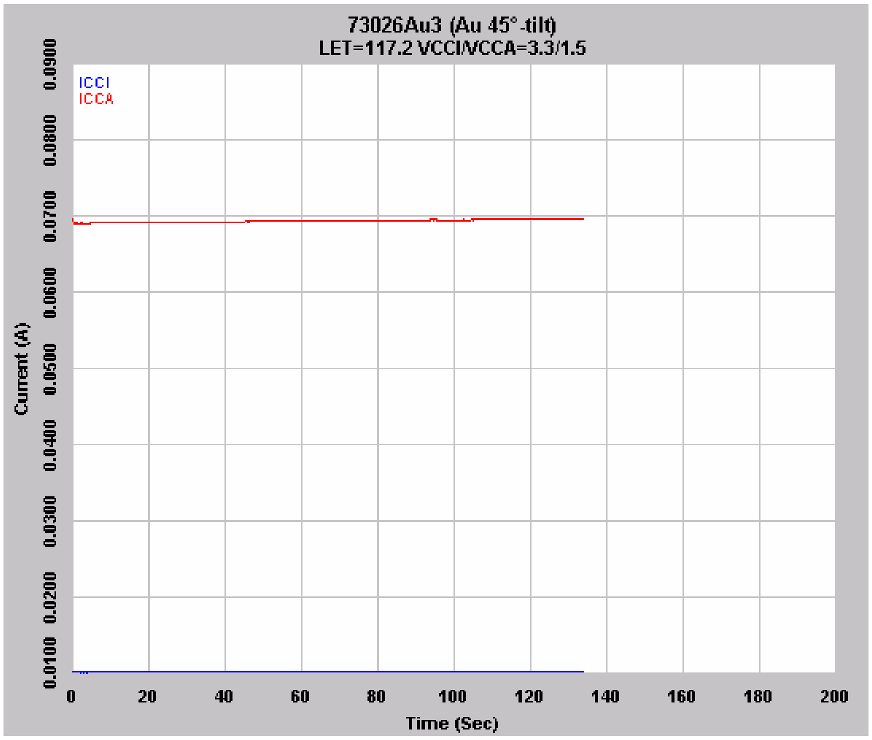

Fig. 3 Plot showing in-flux power supply currents (I_{CCI} and I_{CCA}) of DUT73026 irradiated by Au-ions with 45° tilt; effective LET = 117.2 MeV•cm^2/mg; V_{CCI}/V_{CCA} = 3.3 V/1.5 V.

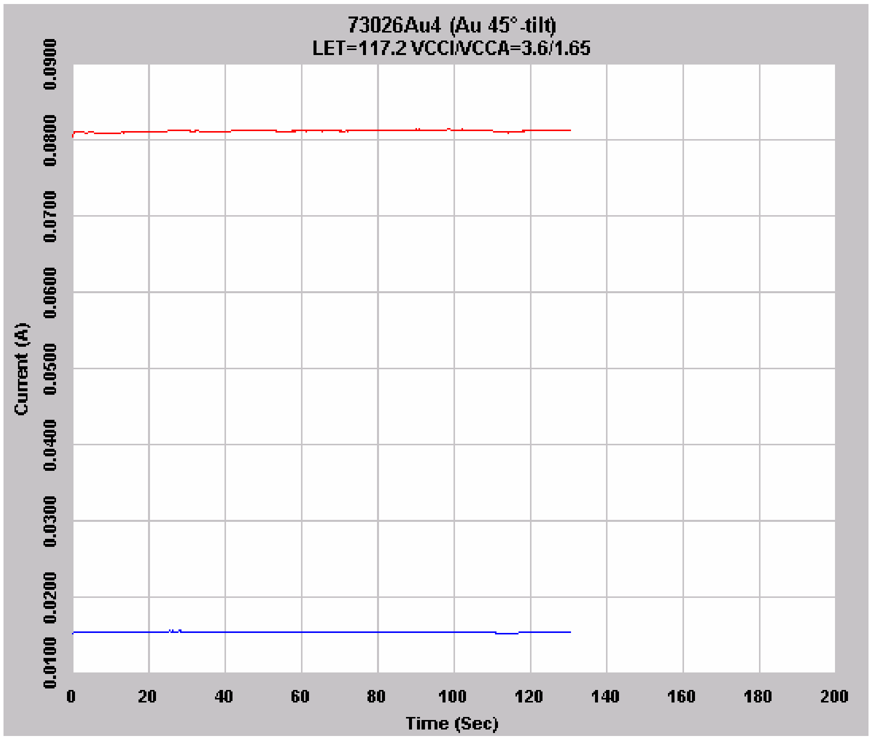

Fig. 4 Plot showing in-flux power supply currents (I_{CCI} and I_{CCA}) of DUT73026 irradiated by Au-ions with 45° tilt; effective LET = 117.2 MeV•cm^2/mg; V_{CCI}/V_{CCA} = 3.6 V/1.65 V.

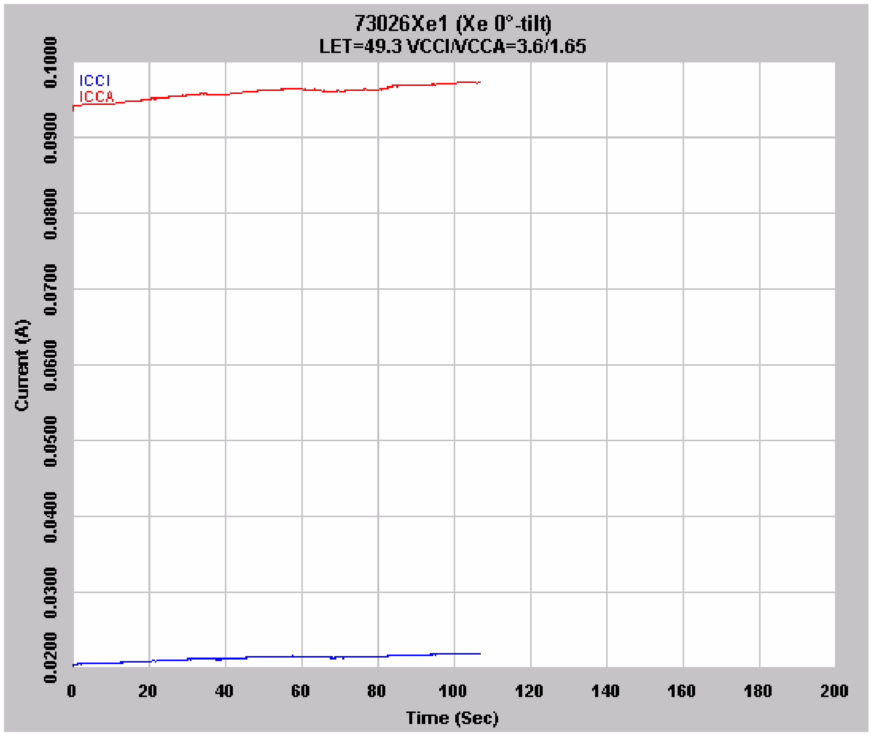

Fig. 5 Plot showing in-flux power supply currents (I_{CCI} and I_{CCA}) of DUT73026 irradiated by Xe-ions with 0° tilt; effective LET = 49.3 MeV•cm^2/mg; V_{CCI}/V_{CCA} = 3.6 V/1.65 V.

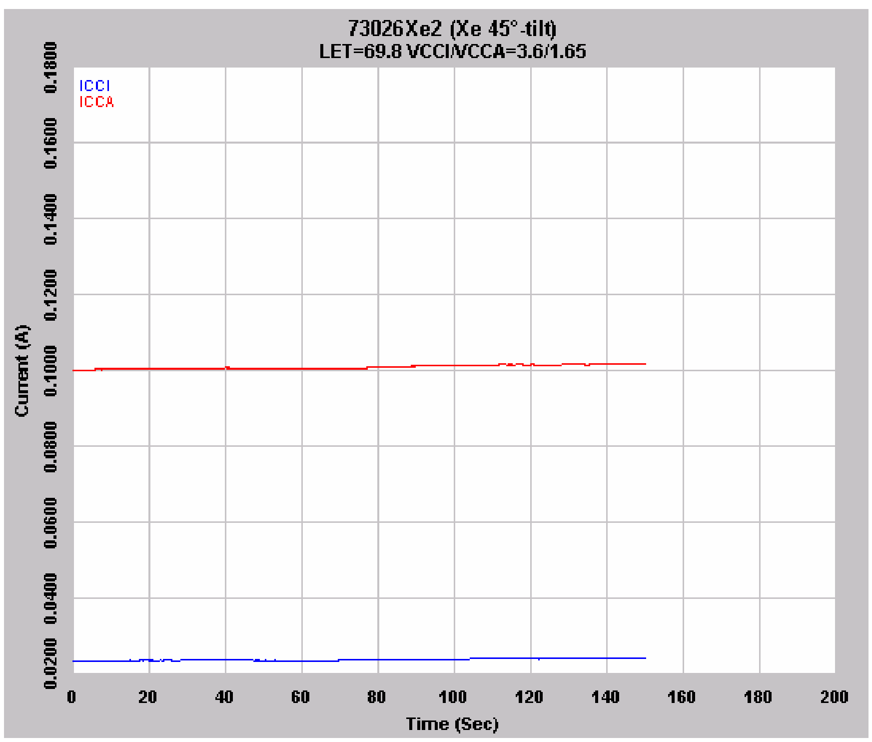

Fig. 6 Plot showing in-flux power supply currents (I_{CCI} and I_{CCA}) of DUT73026 irradiated by Xe-ions with 45° tilt; effective LET = 69.8 MeV•cm^2/mg; V_{CCI}/V_{CCA} = 3.6 V/1.65 V.

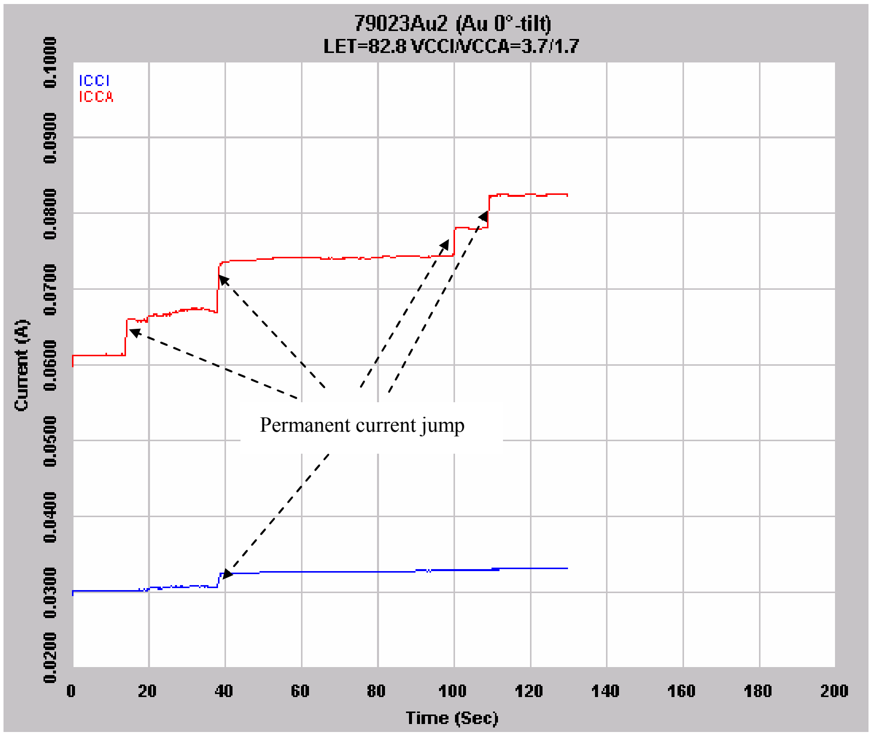

Fig. 7 Plot showing in-flux power supply currents (I_{CCI} and I_{CCA}) of DUT79023 irradiated by Au-ions with 0° tilt; effective LET = 82.8 MeV•cm^2/mg; V_{CCI}/V_{CCA} = 3.7 V/1.7 V.

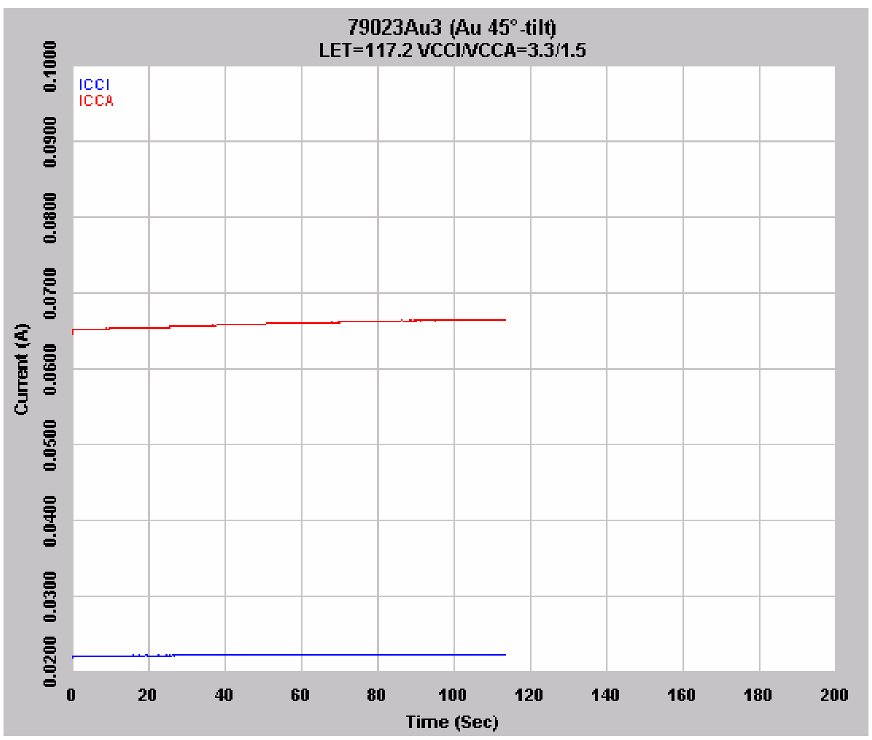

Fig. 8 Plot showing in-flux power supply currents (I_{CCI} and I_{CCA}) of DUT79023 irradiated by Au-ions with 45° tilt; effective LET = 117.2 MeV•cm^2/mg; V_{CCI}/V_{CCA} = 3.3 V/1.5 V.

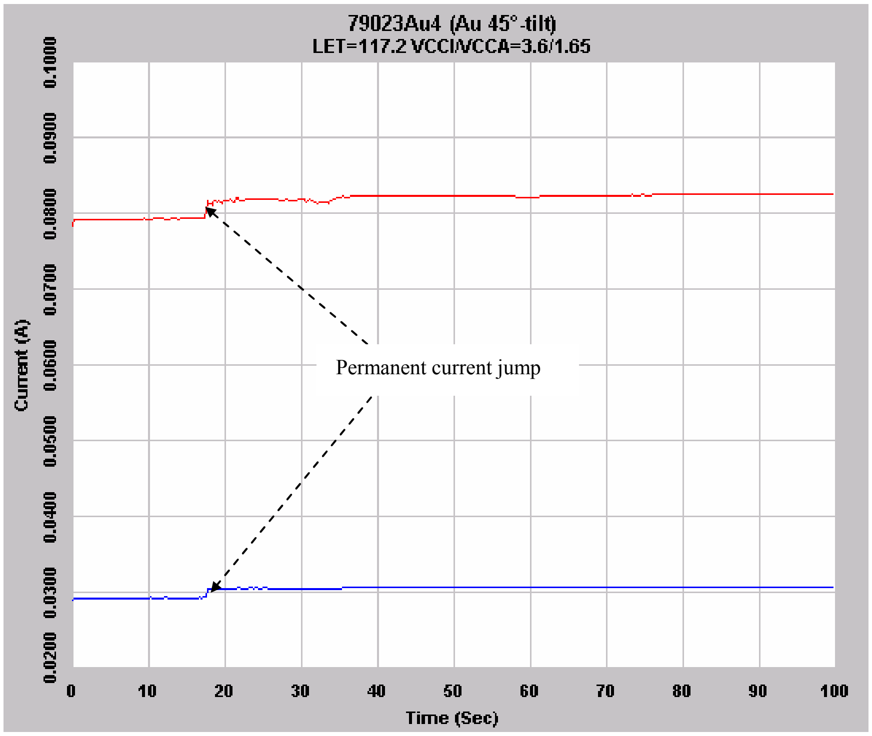

Fig. 9 Plot showing in-flux power supply currents (I_{CCI} and I_{CCA}) of DUT79023 irradiated by Au-ions with 45° tilt; effective LET = 117.2 MeV•cm^2/mg; V_{CCI}/V_{CCA} = 3.6 V/1.65 V.

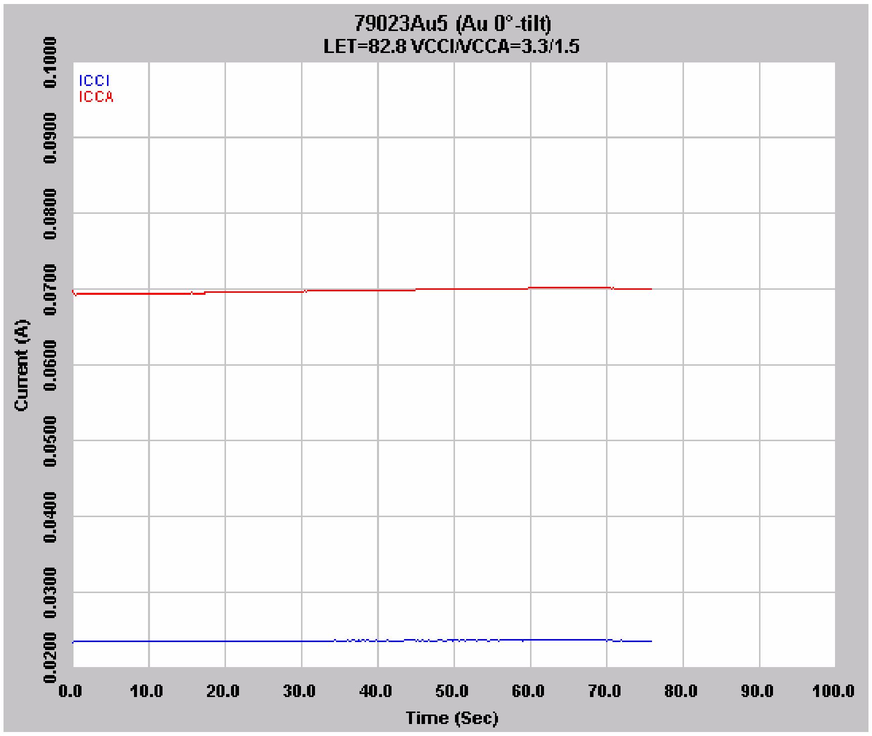

Fig. 10 Plot showing in-flux power supply currents (I_{CCI} and I_{CCA}) of DUT79023 irradiated by Au-ions with 0° tilt; effective LET = 82.8 MeV•cm^2/mg; V_{CCI}/V_{CCA} = 3.3 V/1.5 V.

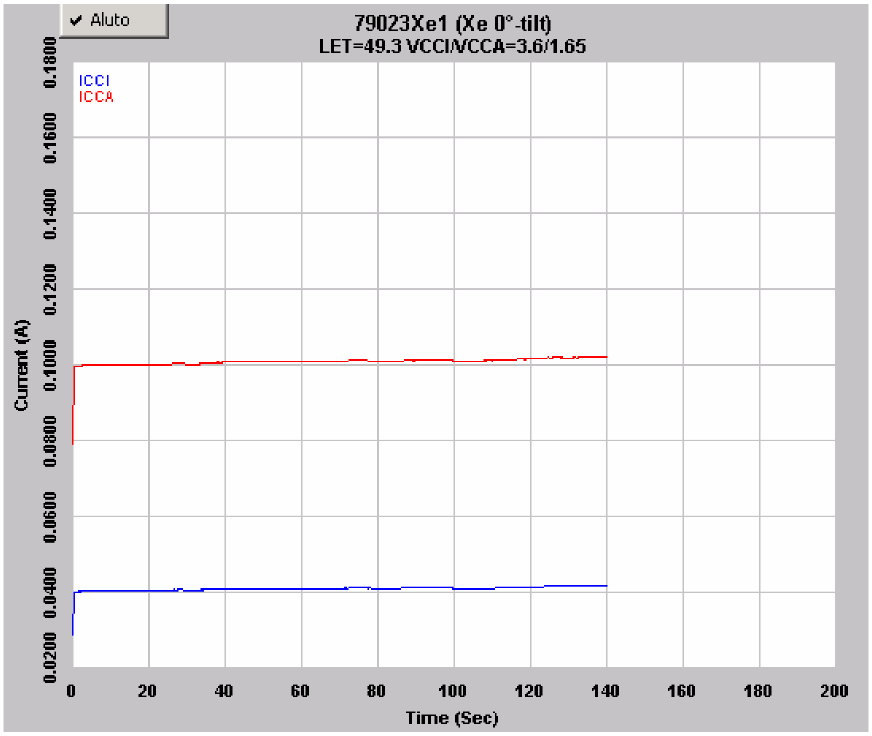

Fig. 11 Plot showing in-flux power supply currents (I_{CCI} and I_{CCA}) of DUT79023 irradiated by Xe-ions with 0° tilt; effective LET = 49.3 MeV•cm^2/mg; V_{CCI}/V_{CCA} = 3.6 V/1.65 V.

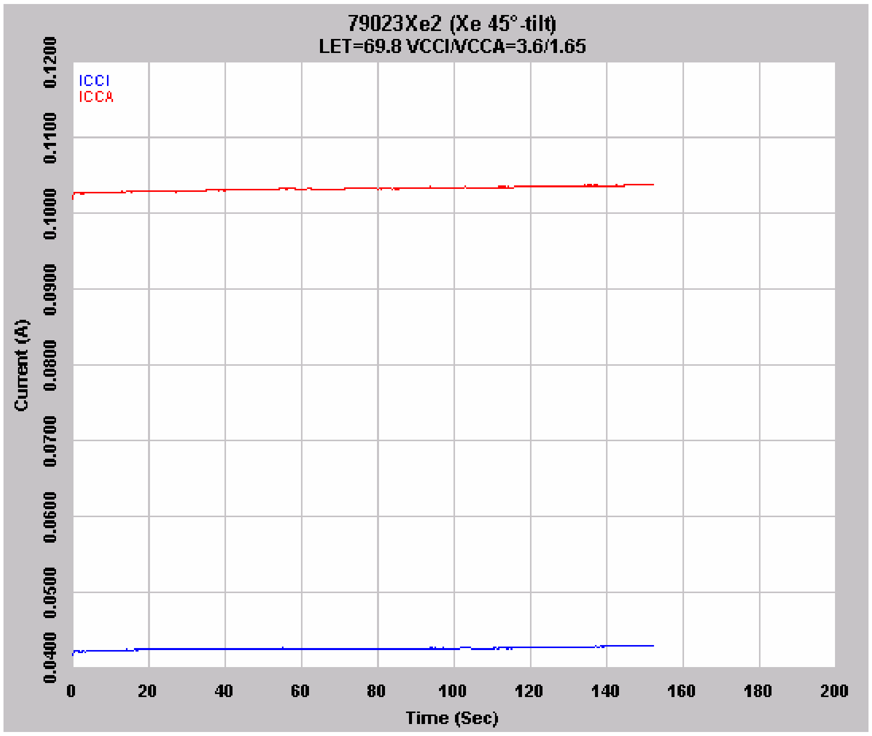

Fig. 12 Plot showing in-flux power supply currents (I_{CCI} and I_{CCA}) of DUT79023 irradiated by Xe-ions with 45° tilt; effective LET = 69.8 MeV•cm^2/mg; V_{CCI}/V_{CCA} = 3.6 V/1.65 V.

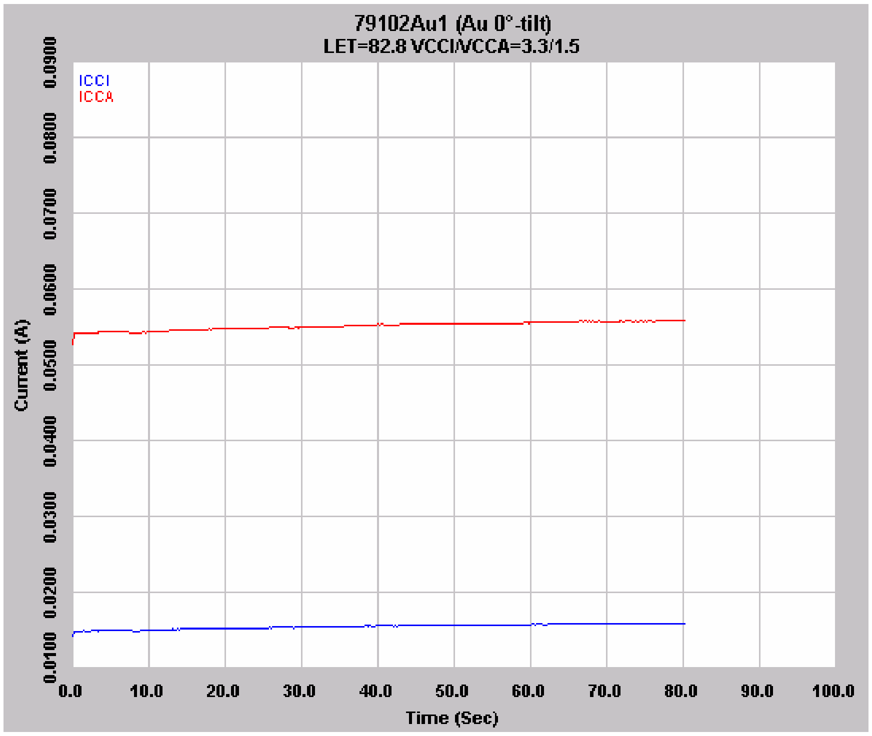

Fig. 13 Plot showing in-flux power supply currents (I_{CCI} and I_{CCA}) of DUT79102 irradiated by Au-ions with 0° tilt; effective LET = 82.8 MeV•cm^2/mg; V_{CCI}/V_{CCA} = 3.3 V/1.5 V.

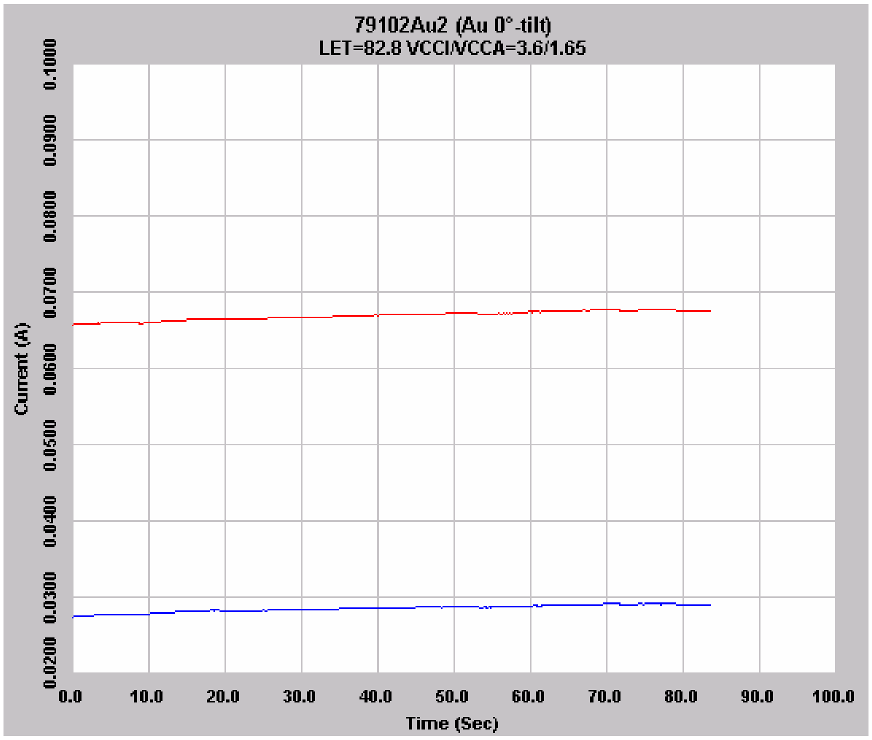

Fig. 14 Plot showing in-flux power supply currents (I_{CCI} and I_{CCA}) of DUT79102 irradiated by Au-ions with 0° tilt; effective LET = 82.8 MeV•cm^2/mg; V_{CCI}/V_{CCA} = 3.6 V/1.65 V.

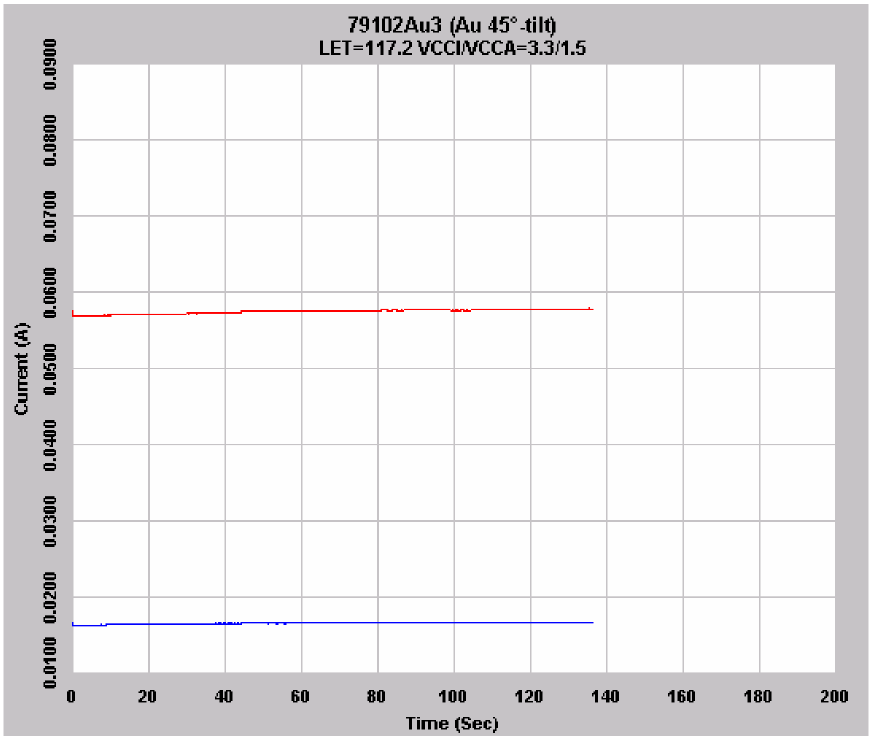

Fig. 15 Plot showing in-flux power supply currents (I_{CCI} and I_{CCA}) of DUT79102 irradiated by Au-ions with 45° tilt; effective LET = 117.2 MeV•cm^2/mg; V_{CCI}/V_{CCA} = 3.3 V/1.5 V.

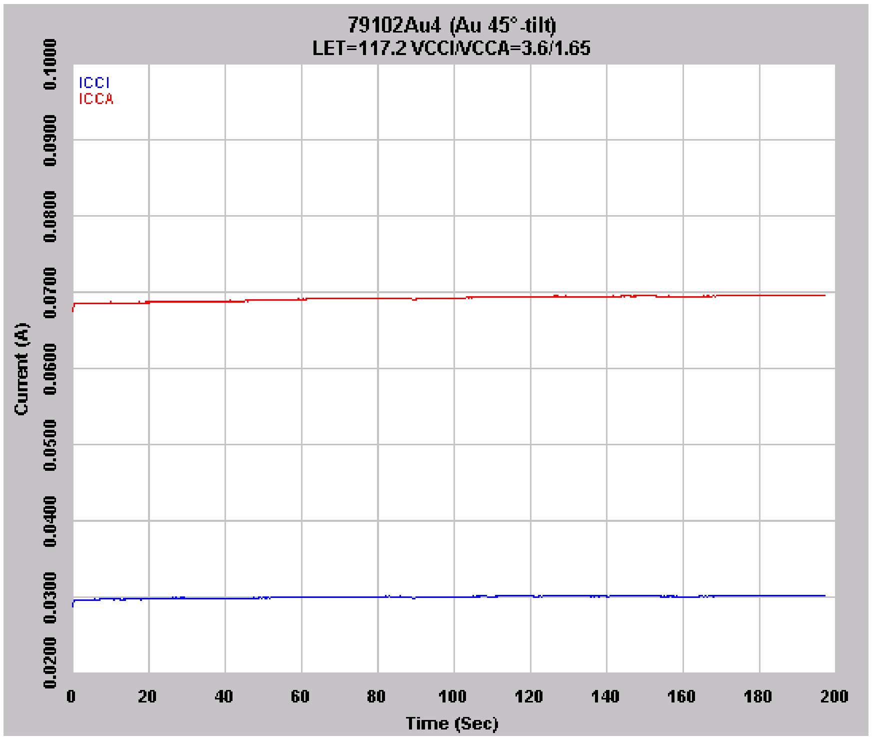

Fig. 16 Plot showing in-flux power supply currents (I_{CCI} and I_{CCA}) of DUT79102 irradiated by Au-ions with 45° tilt; effective LET = 117.2 MeV•cm^2/mg; V_{CCI}/V_{CCA} = 3.6 V/1.65 V.

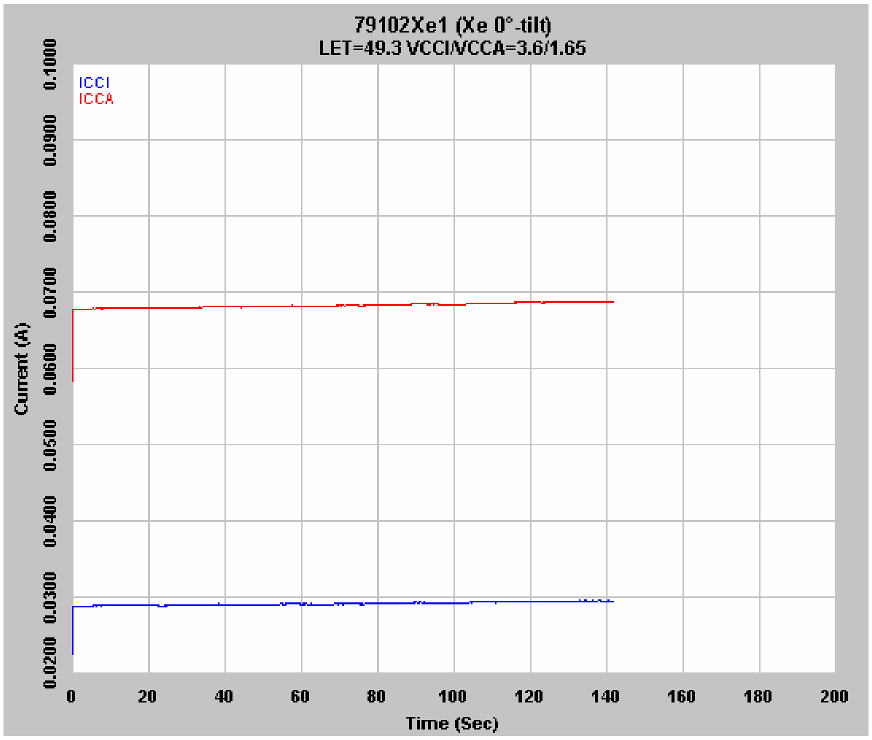

Fig. 17 Plot showing in-flux power supply currents (I_{CCI} and I_{CCA}) of DUT79102 irradiated by Xe-ions with 0° tilt; effective LET = 49.3 MeV•cm^2/mg; V_{CCI}/V_{CCA} = 3.6 V/1.65 V.

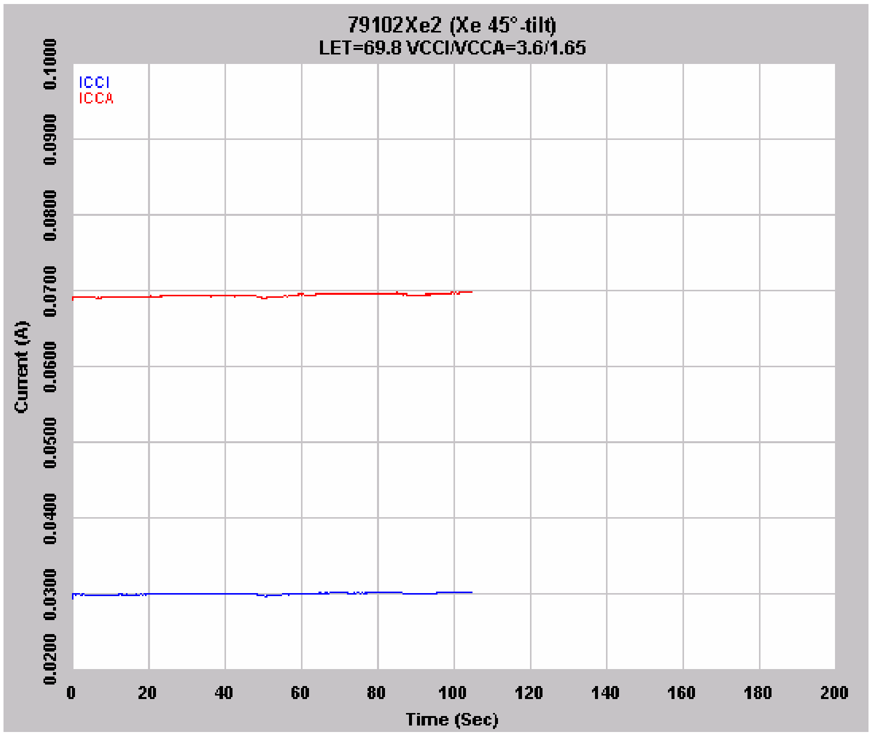

Fig. 18 Plot showing in-flux power supply currents (I_{CCI} and I_{CCA}) of DUT79102 irradiated by Xe-ions with 45° tilt; effective LET = 69.8 MeV•cm^2/mg; V_{CCI}/V_{CCA} = 3.6 V/1.65 V.

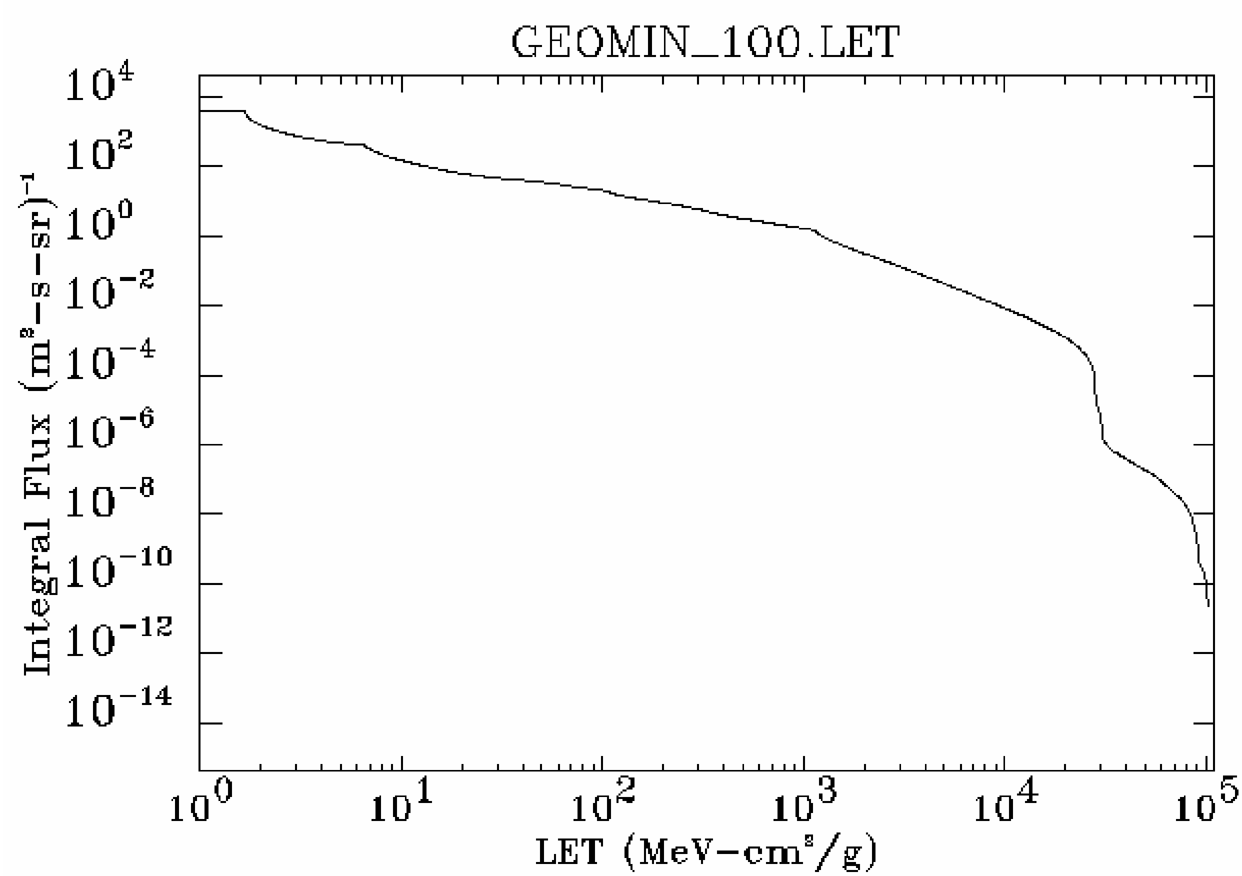

Fig. 19 Plot showing CRÈME96-generated integral flux versus LET in an environment of: geosynchronous orbit, solar minimum, and 100 mil Al shielding.